Discrete elastica

Alfred M. Bruckstein , Robert J. Holt & Arun N. Netravali

Discrete Elastica

ALFRED M. BRUCKSTEIN*, ROBERT J. HOLT and ARUN N. NETRAVALI

Bell Laboratories, Lucent Technologies, Murray Hill, New Jersey 07974

This paper develops a discrete approach to the design of planar curves that minimize cost functions dependent upon their shape. The curves designed by using this approach are piecewise linear with equal length segments and obey various types of endpoint constraints.

1 INTRODUCTION

Planar curves that minimize energy functionals of the form $\int (\alpha \kappa^2 + \beta) ds$, where κ is the curvature and s is arc length, subject to various types of boundary conditions are called elastica, following Euler's 1744 work titled "De Curvis Elastica" [12]. Such curves, also called nonlinear splines in the industrial design context, are important in a variety of applications and have been thoroughly studied in the past by Max Born [2] and A. Love [24]. Recently, due to renewed interest in such curves in computer graphics, CAD, and as shape completion curves in image analysis and computer vision, several papers have appeared, dealing with their effective computation

---

*Permanent address. Department of Computer Science, Technion – IIT 32000, Haifa, Israel

453

and applications; see e.g. [3,5–6,9,11,14,17–19,21–22,25–26,30–31]. Even mathematicians seem to have recently rediscovered these interesting objects [7,15–16,20,23,28]. Since the actual computation of nonlinear splines turns out to be quite difficult, in CAD people turned to simpler polynomial splines or rational curves (NURBS) to address problems of shape design, see e.g. [13,27], and some interesting ideas involving interpolation and design with optimized bi-arc and real algebraic curves which have also appeared [1,29].

In this paper we shall address the problem of designing discretized, piecewise linear curves minimizing functionals of various types that could be regarded as discretized versions of the "curve energy" considered in the context of splines. We shall argue that solving the nonlinear equations that result from considering "discrete elastica" is a feasible alternative to curve design. Furthermore we claim that almost nothing is lost in the process of discretization since it is seldom the case that the differential equations arising from the continuous optimization problem can be explicitly solved. This being the case, those equations must be solved by numerical integration, hence we shall end up with a discretized solution anyhow. We therefore propose to start with a discretized problem and concentrate on numerical procedures that can effectively solve them.

Let us first set the stage for the optimization problems considered. We shall always deal with planar polygonal curves (or poly-lines) with equal-length links (or segments) specified via a set of points $\{\mathbf{P}_i\}_{i=0,1,\dots,N,N+1}$ so that $d(\mathbf{P}_{i+1},\mathbf{P}_i) = l$ for all $i \in \{0,\dots,N\}$ (see Fig. 1).

The turn angle at $\mathbf{P}_i$, defined as $\Psi_i - \Psi_{i-1}$, where Ψ_i is the angle of $\overline{\mathbf{P}_i\mathbf{P}_{i+1}}$ with the x-axis (as in Fig. 1), will be denoted by θ_i, and the curves we shall design will attempt to make these curves as smooth as possible by minimizing an "energy functional" that increases with the increase of these turn angles $|\theta_i|$. In fact the "discrete curvature" at $\mathbf{P}_i$ of a polyline as considered above could be defined as $\kappa_i = \theta_i/l$ and hence a reasonable "energy functional" candidate would be

$$\sum_{i=1}^{N}\left[\alpha\left(\frac{\theta_i}{l}\right)^2 + \beta\right]l \triangleq E_1(\boldsymbol{\theta}, l),$$

where $\boldsymbol{\theta} = \{\theta_1,\dots,\theta_N\}$, mimicking $\int(\alpha\kappa^2 + \beta)ds$ from the continuous case.
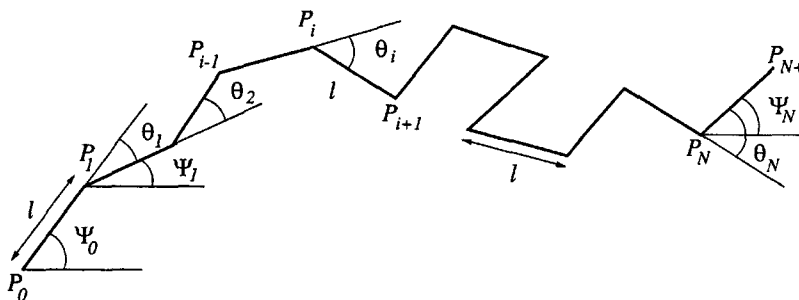
FIGURE 1   A polygonal curve of equal-length segments.

Sometimes one may wish to design curves that are not as smooth as possible but as short as possible for some given boundary conditions, and perhaps some additional restrictions on their curvature; see e.g. Dubins [10]. For such cases we can replace the energy functionals to be optimized with other types of cost functions. Indeed, if, for example, we want to limit the "discrete curvature" of the polylines considered to some $|K|$ we can define a penalty function that increases sharply if the discrete curvature $|\theta/l|$ approaches $|K|$, (for example) as follows:

$$C_{K,m}\left(\frac{\theta}{l}\right) = \left(\frac{\theta}{lK}\right)^{2m}.$$

Here, if m is large, $C_{K,m}(\theta/l)$ becomes huge when $|\theta/l|$ exceeds $|K|$ (see Fig. 2). With such a penalty function we could design curves to optimize

$$E_{K,m}(\theta, l) \triangleq \sum_{i=1}^{N}[\alpha C_{K,m}(\theta_i/l) + \beta]l \tag{1}$$

for given boundary conditions.

Boundary conditions that will be of interest to us here are the origin and endpoint of the polygonal curves and the directions of the first and last links. We shall assume that the first link starts at $(0,0)$ in the plane and the last link ends at some $(L,0)$, clearly without
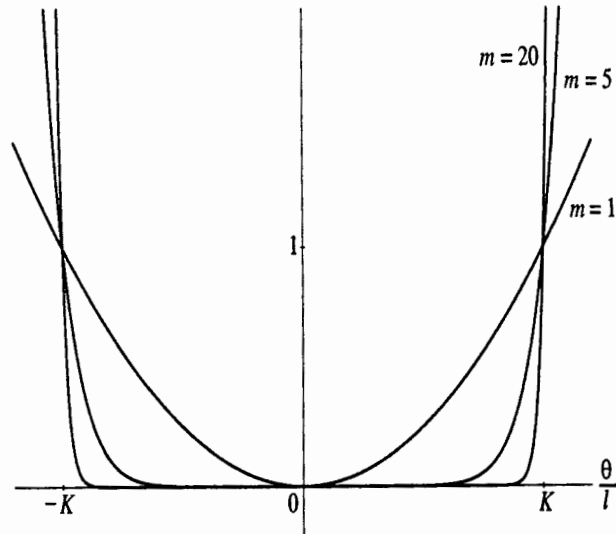
FIGURE 2   The function $C_{K,m}(\theta/l) = [\theta/(lK)]^{2m}$ for different values of m.

any loss of generality, since we would like to have at least Euclidean invariance built into the design process! Moreover, since we shall sometimes aim to have similarity (i.e. scale) invariance, we may also allow l and/or L to vary freely, according to the case.

Next we shall examine several cases of discrete elastica designs. Those will include solving the following type of optimization problem:

minimize $E(\theta, l)$ subject to: predetermined Ψ_0 and Ψ_N

$$\sum_{i=0}^{N} l \cos \Psi_i = L$$

$$\sum_{i=0}^{N} l \sin \Psi_i = 0,$$

where $\Psi_j \triangleq \Psi_0 + \sum_{i=1}^{j} \theta_i$ for $j = 1, \ldots, N$. There are several parameters in such optimization problems that can be either set a priori or optimized. The number of links $N + 1$ and the length of each link (jointly determining the length of the curve as $(N + 1)l$) are such parameters. L is also free if we are interested in similarity invariant elastica, since it scales directly with l.

2. "CLASSICAL" DISCRETE ELASTICA

We shall first discuss polygonal elastica (poly-elastica) that minimize

$$E(\theta, l) = \sum_{i=1}^{N} \left[\alpha \left(\frac{\Psi_i - \Psi_{i-1}}{l} \right)^2 + \beta \right] l \tag{1}$$

subject to

$$\Psi_0 \text{ and } \Psi_N \text{ predetermined}$$

$$\sum_{i=0}^{N} l \cos \Psi_i = L$$

$$\sum_{i=0}^{N} l \sin \Psi_i = 0.$$

Using the Lagrange multiplier technique we consider the cost function

$$\mathcal{G}(\Psi, \lambda_1, \lambda_2, l; L, N, \alpha, \beta) = \sum_{i=1}^{N} \left[\alpha \left(\frac{\Psi_i - \Psi_{i-1}}{l} \right)^2 + \beta \right] l + \lambda_1$$

$$\times \left[\sum_{i=0}^{N} l \cos \Psi_i - L \right] + \lambda_2 \left[\sum_{i=0}^{N} l \sin \Psi_i \right].$$

where Ψ denotes the vector of unknown angles $\{\Psi_1, \ldots, \Psi_{N-1}\}$. Taking derivatives with respect to the $N + 2$ variables $\Psi_1, \ldots, \Psi_{N-1}$, λ_1, λ_2, and l, leads to the system of equations

$$\left. \begin{aligned} \frac{2\alpha(-\Psi_{j-1} + 2\Psi_j - \Psi_{j+1})}{l^2} - \lambda_1 \sin \Psi_j + \lambda_2 \cos \Psi_j = 0, \quad j = 1, \ldots, N - 1, \\ l \sum_{i=0}^{N} \cos \Psi_i - L = 0, \qquad \sum_{i=0}^{N} \sin \Psi_i = 0, \\ -\alpha \sum_{i=1}^{N} \left(\frac{\Psi_i - \Psi_{i-1}}{l} \right)^2 + N\beta + \lambda_1 \sum_{i=0}^{N} \cos \Psi_i + \lambda_2 \sum_{i=0}^{N} \sin \Psi_i = 0. \end{aligned} \right\}$$

$$\tag{2}$$

2.1 Numerical Experiments with Euclidean-invariant Elastica

In this subsection we discuss the numerical solutions corresponding to the cost function. We also show several families of curves illustrating how changing some of the parameters affects the minimal cost curves for the various cost functions.

The discrete Euclidean-invariant elastica curves are solutions of the optimization problem (1). The solutions are found by solving the system (2), and this was accomplished by using the technique discussed for the turn/curvature limited elastica in Section 5.3 and substituting in $K = 1$ and $m = 1$. The program was written with the symbolic manipulation program Maple [8], and uses the Newton–Raphson method directly on the system (2).

Figure 3 shows the effect on varying the terminal angle while holding the other parameters constant at $\Psi_0 = 135°$, $L = 10$, $N = 32$, $\alpha = 1$, $\beta = 1$.

Figure 4 shows the effect of α and β on the results. As the ratio β/α increases, the contribution of the length of the curve to the cost function increases, and as a result the length of the curve decreases. This phenomenon is readily seen in Fig. 4, which shows curves for $\beta/\alpha = 0.1, 1.0$, and 10. The other parameters are fixed at $\Psi_0 = 180°$, $\Psi_N = 180°$, $L = 10$, and $N = 32$.

Figure 5 shows the effect on varying N, one less than the number of links, while holding the other parameters constant at $\Psi_0 = 45°$, $\Psi_N = -135°$, $L = 6$, $\alpha = 1$, $\beta = 1$. There is very little change in the curve for values of N larger than 64.
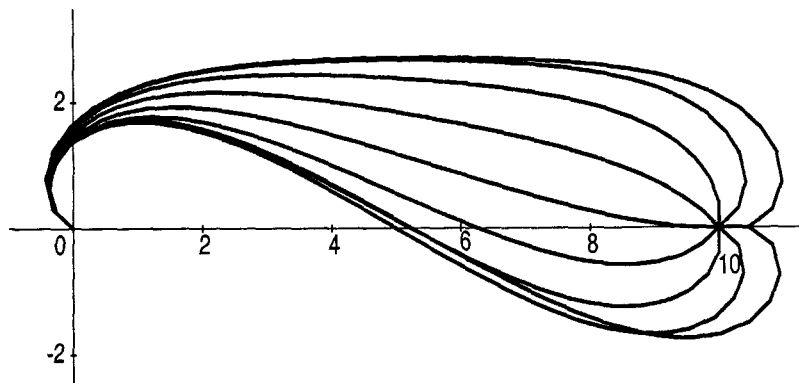
FIGURE 3   Discrete Euclidean elastica with $\Psi_0 = 135°$, $\Psi_N = -180°, -135°, \ldots, 180°$.
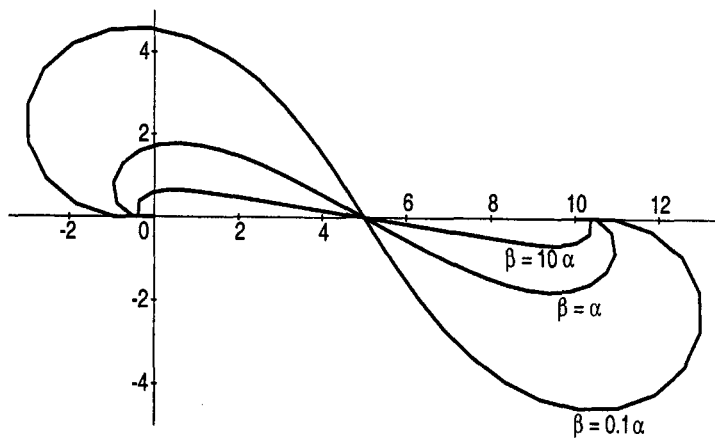
FIGURE 4   Discrete Euclidean elastica with $\Psi_0 = 180°, \Psi_N = 180°$, and $\beta/\alpha =$ 0.1, 1, 10.
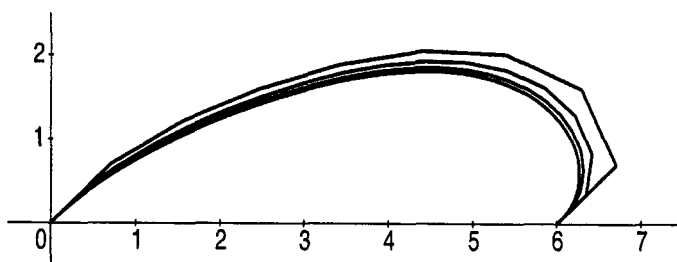
FIGURE 5   Discrete Euclidean elastica with varying N. From top to bottom at $x = 5$, these are the curves for $N = 8, 16, 32$, and 64 respectively.

3 SIMILARITY-INVARIANT ELASTICA

The above case addresses the problem of design of polylines that allows the boundary conditions to set/choose an optimal link-length l. We could, however, address a different type of optimization too: we could set $l = 1$ and let the endpoint $(L, 0)$ be free to settle anywhere on the positive x-axis. Indeed we can readily imagine a "discrete" physical spline made from inelastic sections, or links, of length 1, connected with elastic joints where the bending potential energy depends on the turn angle θ as $\alpha\theta^2$. The problem we would address in this case would be to determine the lowest energy configuration

of such a "spline" when the first link is forced to make an angle of Ψ_0 with the x-axis and the last link an angle of Ψ_N with its endpoint free to slide along the positive x-axis (see Fig. 6).

With $l = 1$ we have the following optimization problem:

$$\text{minimize } E(\theta, l) = \sum_{i=1}^{N}(\Psi_i - \Psi_{i-1})^2$$

$$\text{subject to } \sum_{i=0}^{N}\sin\Psi_i = 0 \tag{3}$$

$$\sum_{i=0}^{N}\cos\Psi_i > 0.$$

Again, Lagrange multipliers were used to form the expression

$$\mathcal{F}(\Psi, \lambda; N) = \sum_{i=1}^{N}(\Psi_i - \Psi_{i-1})^2 + \lambda \sum_{i=0}^{N}\sin\Psi_i,$$

where Ψ denotes the vector of unknown angles $\{\Psi_1, \ldots, \Psi_{N-1}\}$. Taking derivatives with respect to the N variables $\Psi_1, \ldots, \Psi_{N-1}$, and λ leads to the system of equations

$$\left.\begin{array}{l} 2(-\Psi_{j-1} + 2\Psi_j - \Psi_{j+1}) + \lambda\cos\Psi_j = 0, \quad j = 1, \ldots, N-1, \\ \displaystyle\sum_{i=0}^{N}\sin\Psi_i = 0. \end{array}\right\} \tag{4}$$

Rewriting the first equation in (4), we recognize that this discrete minimization problem leads to the two point boundary value problem

$$\Psi_{i+1} = 2\Psi_i + \frac{\lambda}{2}\cos\Psi_i - \Psi_{i-1}, \quad i = 1, \ldots, N-1,$$

where Ψ_0 and Ψ_N are given. Note that in this case the total length of the discrete spline is *a priori* (implicitly) set to $(N + 1) \cdot l = N + 1$.

This optimization problem was considered in [3], and solved via a shooting method. It represents a discrete version of a scale-invariant version of minimal energy curves. Indeed, it was proved in [3] that
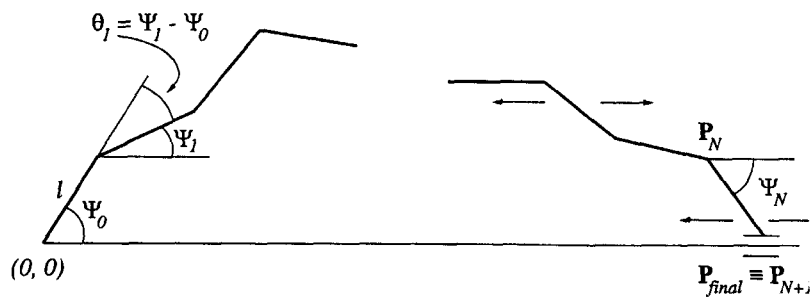
FIGURE 6   The terminal point may "slide" along the x-axis.

$\int ds \cdot \int \kappa^2 ds$ is a scale-invariant energy measure that leads to circular interpolations for symmetric endpoint conditions, a very desirable property indeed.

The main motivation for introducing the modified energy functional in [3] was the consideration of a counterintuitive result of Horn asserting that the least energy curve (minimizing $\int \kappa^2 ds$) which starts vertically up at $(0,0)$ and arrives vertically down at $(1,0)$ is not a semicircle [17]. This result is due to the use of a cost function that does not penalize the curve length and is not scale invariant. Later, Moreton and Séquin also realized the advantage of similarity invariant cost functionals based on curvature and curvature variation in the design of curves, see [26]. The cost functions proposed by them were $\int \kappa^2 ds$ and $\int (d\kappa/ds)^2 ds$ for Euclidean invariant elastica and $(\int ds \cdot \int \kappa^2 ds)$, as in [3], and $(\int ds)^3 (\int (d\kappa/ds)^2 ds)$ for scale invariant versions. We shall briefly return to some minimal variation curve design ideas in a later section.

3.1 Numerical Experiments with Similarity-invariant Elastica

As in [3], we are interested here in solutions of the minimization problem (3). Another program using Maple was written to solve this problem, specifically the system (4), for a wide range of parameter values. These were solved by using the technique for the "similarity-invariant" curvature limited elastica discussed in detail in Section 5.4 and substituting in $K = 1$, $m = 1$, $\alpha = 1$, and $\beta = 0$.

Figure 7 shows the effect on varying the terminal angle while holding the other parameters constant at $\Psi_0 = 135°$, $N = 32$.
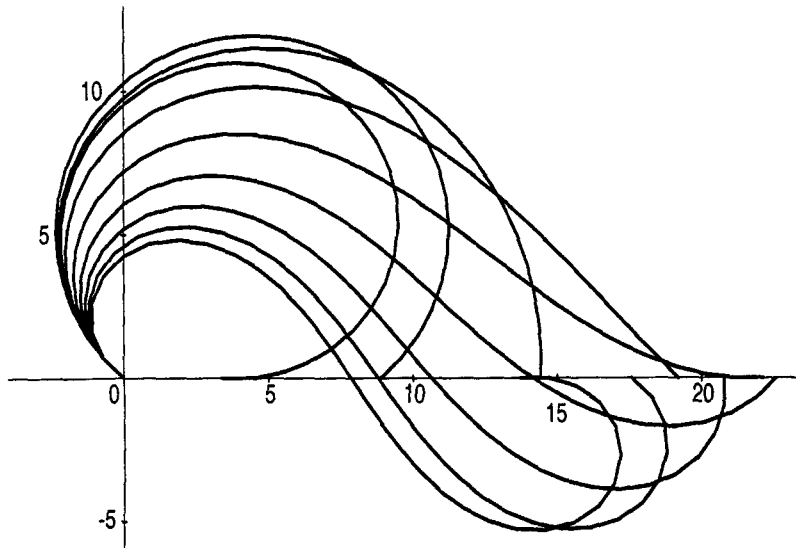
FIGURE 7   Discrete similarity-invariant elastica with $N = 32$, $\Psi_0 = 135°$, $\Psi_N = -180°, -135°, \ldots, 180°$.

Figure 8 shows the same results as in Fig. 7, but with all of the distances scaled so that $L = x_{N+1} = 1$. This has the effect of changing the length of each link from 1 to $1/x_{N+1} = 1/\sum_{i=0}^{N} \cos \Psi_i$.

Figure 9 shows the effect on varying N, one less than the number of links, while holding the other parameters constant at $\Psi_0 = 45°$ and $\Psi_N = -135°$.

Figure 10 shows the same results as in Fig. 9, but with all of the distances scaled so that $x_{N+1} = 1$. The curves converge to a smooth path as N increases. The limiting curve is not of circle–line–circle type since $m = 1$ here; the circle–line–circle behavior appears only for large m.

4   DISCRETE ELASTICA WITH HARD LIMITS ON TURN

In this section we address the problem of optimizing interpolation curves for other types of cost functions. In particular we shall be interested in penalizing curvatures in such a way that the resulting polylines will have turns, or "discrete curvatures," limited to an *a priori* given range. To obtain this result we can solve for polygonal elastica that
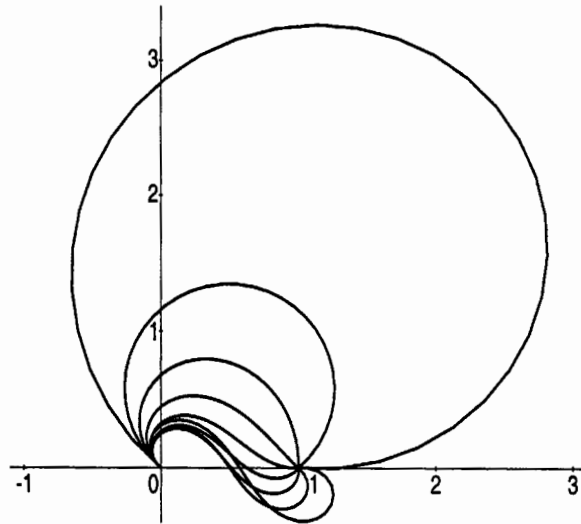
FIGURE 8   Normalized similarity-invariant elastica with $N = 32$, $\Psi_0 = 135°$, $\Psi_N = -180°, -135°, \ldots, 180°$.
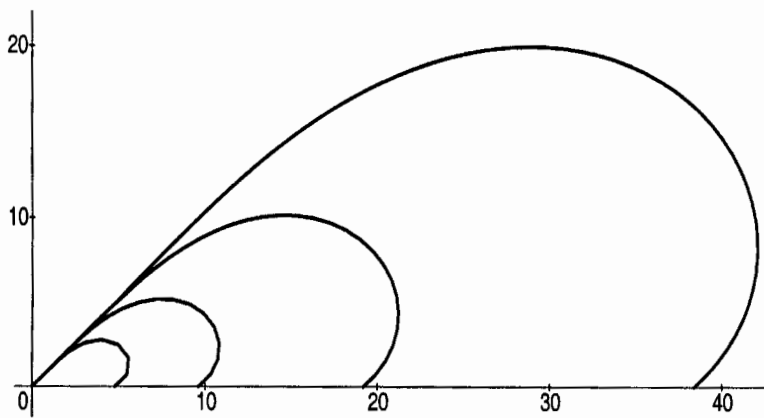
FIGURE 9   Similarity-invariant elastica with varying N. In order of increasing length, these are the curves for $N = 8, 16, 32$, and 64 respectively.

minimize, say

$$E_{K,m}(\boldsymbol{\theta}, l) = \sum_{i=1}^{N}\left[\alpha\left(\frac{\Psi_i - \Psi_{i-1}}{lK}\right)^{2m} + \beta\right]l \qquad (5)$$
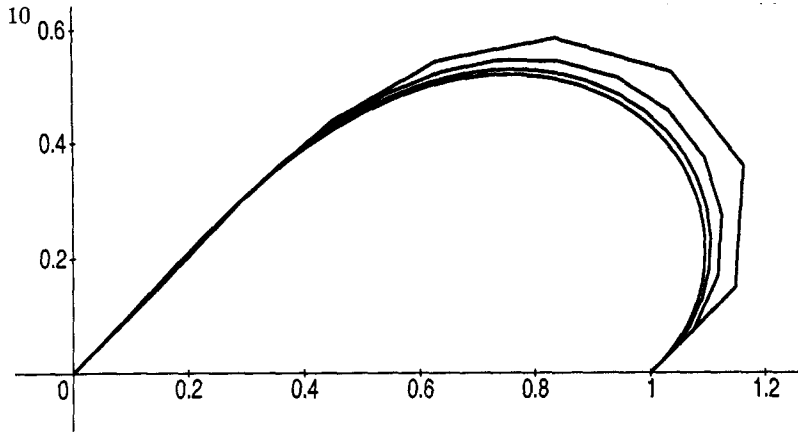
FIGURE 10 Normalized similarity-invariant elastica with varying N. From top to bottom at $x = 0.8$, these are the curves for $N = 8, 16, 32$, and 64 respectively.

subject to the same conditions as before. The Lagrange approach leads here to a nonlinear system of equations that displays the necessary condition for optimality, i.e.

$$\mathcal{G}(\Psi, \lambda_1, \lambda_2, l; K, L, m, N, \alpha, \beta)$$

$$= \sum_{i=1}^{N} \left[\alpha \left(\frac{\Psi_i - \Psi_{i-1}}{lK} \right)^{2m} + \beta \right] l + \lambda_1 \left[\sum_{i=0}^{N} l \cos \Psi_i - L \right] + \lambda_2 \left[\sum_{i=0}^{N} l \sin \Psi_i \right].$$

Taking derivatives with respect to the $N + 2$ variables $\Psi_1, \ldots, \Psi_{N-1}$, λ_1, λ_2, and l, leads to the following system of nonlinear equations generalizing (2):

$$\left. \begin{array}{c} \dfrac{2m\alpha[(\Psi_j - \Psi_{j-1})^{2m-1} - (\Psi_{j+1} - \Psi_j)^{2m-1}]}{(lK)^{2m}} - \lambda_1 \sin \Psi_j + \lambda_2 \cos \Psi_j = 0, \\[2mm] j = 1, \ldots, N-1, \\[2mm] l \sum_{i=0}^{N} \cos \Psi_i - L = 0, \quad \sum_{i=0}^{N} \sin \Psi_i = 0, \\[2mm] -(2m-1)\alpha \sum_{i=1}^{N} \left(\dfrac{\Psi_i - \Psi_{i-1}}{lK} \right)^{2m} + N\beta + \lambda_1 \sum_{i=0}^{N} \cos \Psi_i + \lambda_2 \sum_{i=0}^{N} \sin \Psi_i = 0. \end{array} \right\}$$

$$(6)$$

Note that if $(\Psi^*, \lambda_1^*, \lambda_2^*, l^*)$ is a solution for the set of parameters $(K, L, m, N, \alpha, \beta)$, then $(\Psi^*, \lambda_1^*, \lambda_2^*, cl^*)$ is a solution for the set of parameters $(K/c, cL, m, N, \alpha, \beta)$. Thus the solution curve scales with L as long as LK is held constant.

Consequently we shall have for Ψ_j the following system of nonlinear equations:

$$
\Psi_{j+1} = \Psi_j + \left[(\Psi_j - \Psi_{j-1})^{2m-1} + \frac{(2m-1)\sum_{i=1}^{N}(\Psi_i - \Psi_{i-1})^{2m}}{2m\left(N\beta + \lambda_1 \sum_{i=0}^{N}\cos\Psi_i + \lambda_2 \sum_{i=0}^{N}\sin\Psi_i\right)} \right.
$$
$$
\left. \times (\lambda_2 \cos\Psi_j - \lambda_1 \sin\Psi_j) \right]^{1/(2m-1)} \qquad j = 1, \dots, N,
$$

with λ_1 and λ_2 to be determined so as to obey the conditions $\sum_{i=0}^{N} \sin\Psi_i = 0$ and $\sum_{i=0}^{N} l\cos\Psi_i = L > 0$. Note that l and K (or L and K) scale so that all solutions for which LK equal a constant are similar up to a scaling parameter!

4.1 Numerical Experiments on Curvature Hard-limited Elastica

As we saw in Section 4, here we want to solve the minimization problem (5). We wrote another Maple program to solve the system (6) for many parameter values. The system of equations was solved using the Newton–Raphson method with an initial guess close to the solution for the continuous case, as suggested by [10]. That is, an approximation to a circle–line–circle type curve that meets the required boundary conditions is first found as follows. There are two generic cases: that in which the line segment is an interior tangent to the two circles and that in which the segment is an exterior tangent. Due to symmetry about the x-axis, we can assume that $\Psi_0 \geq 0$. The first case arises when Ψ_N is also nonnegative. This situation is depicted in Fig. 11. In this figure C_1 and C_2 are circles of radius $R = 1/K$, $\overline{C_1 D}$ and $\overline{C_2 E}$ are vertical line segments, P_0 is $(0, 0)$, and P_N is $(L, 0)$. $\overline{AB}$ is the interior tangent, and A has coordinates $(R(\sin\Psi_0 + \sin\alpha), R(-\cos\Psi_0 + \cos\alpha))$, B has coordinates $(L - R(\sin\Psi_N + \sin\alpha), R(\cos\Psi_N - \cos\alpha))$, C_1 is $(R\sin\Psi_0, -R\cos\Psi_0)$,
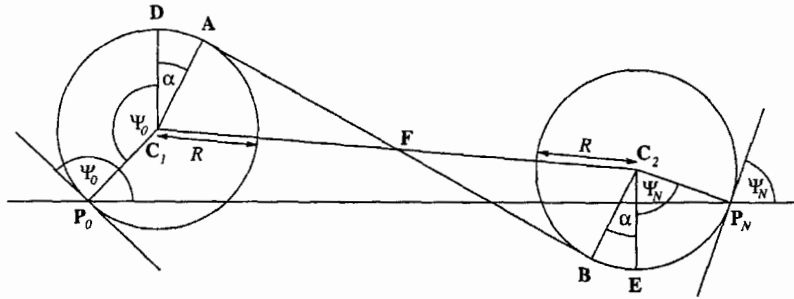
FIGURE 11   Geometry when $\Psi_N \geq 0$. The circle-line-circle path consists of arc P_0DA, segment AB, and arc BEP_N.

C_2 is $(L - R\sin\Psi_N, R\cos\Psi_N)$, and F is $([L - R(\sin\Psi_N - \sin\Psi_0)]/2,$ $R(\cos\Psi_N - \cos\Psi_0)/2)$.

Triangle $\Delta C_1 AF$ is a right triangle, and by the Pythagorean Theorem we obtain

$$4R^2 + [L - R(\sin\Psi_0 + \sin\Psi_N - 2\sin\alpha)]^2 + R^2(\cos\Psi_0 + \cos\Psi_N - 2\cos\alpha)^2$$
$$= [L - R(\sin\Psi_0 + \sin\Psi_N)]^2 + R^2(\cos\Psi_0 + \cos\Psi_N)^2,$$

which simplifies to

$$[L - R(\sin\Psi_0 + \sin\Psi_N)]\sin\alpha + R(\cos\Psi_0 + \cos\Psi_N)\cos\alpha - 2R = 0.$$

From this we obtain

$$\tan\alpha = \frac{-bc + e\sqrt{b^2 + c^2 - e^2}}{b^2 - e^2},$$

where

$$b = L - R(\sin\Psi_0 + \sin\Psi_N), \quad c = R(\cos\Psi_0 + \cos\Psi_N), \quad e = 2R.$$

Having determined α, the length of the circle–line–circle path is found to be

$$R(\Psi_0 + \Psi_N + 2\alpha)$$
$$+ \sqrt{L^2 - 2LR + 2R^2[3 + \cos(\Psi_0 - \Psi_N) - 2\cos(\Psi_0 + \alpha) - 2\cos(\Psi_N + \alpha)]},$$

so the initial guess for l, call it l_0, is this length divided by $N + 1$, the number of links in the polyline. The slope of the segment piece is

$$\frac{R(\cos \Psi_0 + \cos \Psi_N - 2 \cos \alpha)}{L - R(\sin \Psi_0 + \sin \Psi_N + 2 \sin \alpha)},$$

and we can let γ be the arctangent of this quantity. As long as $L > 4R$, γ will have a value between $-\pi/2$ and 0. For smaller values of L, the circles centered at C_1 and C_2 may intersect, and then the optimal path will take on a different structure, with the path having to travel far away from the circles in order to satisfy the boundary conditions. This case is of less practical interest, since it involves curves whose length is much greater than the distance between the terminal points.

The initial value of Ψ_1 is chosen to be slightly more than $\Psi_0 - l_0 K$, as turns less than $l_0 K$ are not penalized heavily by the cost function $G(\Psi, \lambda_1, \lambda_2, l; K, L, m, N, \alpha, \beta)$. Then the initial value of Ψ_i is chosen as slightly more than $\Psi_0 - i l_0 K$ for $i = 1, 2, \ldots$, until this quantity is less than γ. Coming from the other end, Ψ_{N-1} is initially chosen as slightly more than $\Psi_N - l_0 K$, and Ψ_{N-i} is taken as slightly more than $\Psi_N - i l_0 K$ for $i = 1, 2, \ldots$, until this is smaller than γ. Ψ_i is set equal to γ for the remaining values of i.

We next discuss the case where the straight line segment portion is an exterior tangent to the two circles. This case arises when Ψ_N is nonpositive and Ψ_0 is nonnegative, and is depicted in Fig. 12. In this figure, as in Fig. 11, C_1 and C_2 are circles of radius $R = 1/K$, $\overline{C_1 D}$ and $\overline{C_2 E}$ are vertical line segments, P_0 is $(0, 0)$, and P_N is $(L, 0)$. Here we have $\overline{AB}$ is the exterior tangent, and A has coordinates $(R(\sin \Psi_0 - \sin \alpha), R(-\cos \Psi_0 + \cos \alpha))$, B has coordinates $(L - R(-\sin \Psi_N + \sin \alpha), R(\cos \Psi_N + \cos \alpha))$, C_1 is $(R \sin \Psi_0, -R \cos \Psi_0)$, and C_2 is $(L + R \sin \Psi_N, -R \cos \Psi_N)$.

The situation here is simpler than in the previous case, for here arcs with angle α cancel. That is, the length of the curved portion is $R(\Psi_0 - \alpha) + R(-\Psi_N + \alpha) = R(\Psi_0 - \Psi_N)$. The length of the straight portion equals the distance between the two centers, and thus the total length of the path is

$$R(\Psi_0 - \Psi_N) + \sqrt{L^2 - 2RL(\sin \Psi_0 - \sin \Psi_n) + 2R^2[1 - \cos(\Psi_0 - \Psi_N)]}.$$
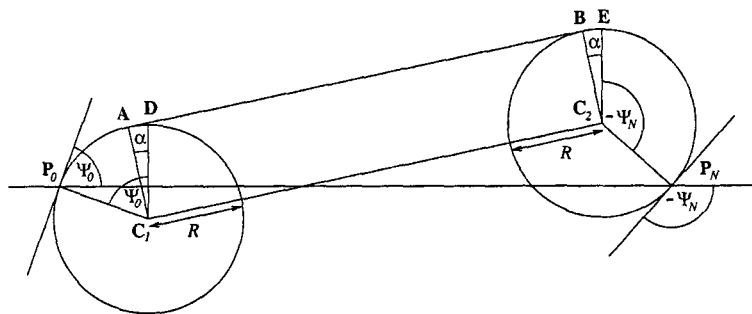
FIGURE 12 Geometry when $\Psi_N \leq 0$. The circle-line-circle path consists of arc P_0A, segment AB, and arc BEP_N.

This time the initial value l_0 is this length divided by $N + 1$, and the slope of the segment piece is

$$\tan \gamma = \frac{R(\cos \Psi_0 - \cos \Psi_N)}{L - R(\sin \Psi_0 - \sin \Psi_N)}.$$

The procedure for choosing the initial values of the Ψ_i is similar to that of the previous case. The initial value of Ψ_i is chosen as slightly more than $\Psi_0 - il_0K$ for $i = 1, 2, \ldots$, until this quantity is less than γ. However, in this case, Ψ_{N-1} is initially chosen as slightly less than $\Psi_N + l_0K$, and Ψ_{N-i} is taken as slightly less than $\Psi_N + il_0K$ for $i = 1, 2, \ldots$, until this is greater than γ. Ψ_i is set equal to γ for the remaining values of i.

The value of $-\beta$ was chosen as the initial guess for λ_1 on the grounds that in a solution of (6), each of the terms $[(\Psi_i - \Psi_{i-1})/(lK)]^{2m}$ is likely to be small, $\sum_{i=0}^{n} \cos \Psi_i$ will equal $L/l \approx N$ for N large, and $\sum_{i=0}^{n} \sin \Psi_i$ will be zero. The quantity λ_2 was usually found to be a small positive number, so we just used an initial value of zero for that.

We went to this much trouble obtaining a good initial guess so that the Newton–Raphson method will converge to the correct answer, and in not a large number of iterations. In most of the examples fewer than ten iterations were required.

Figure 13 shows the effect on varying the terminal angle while holding the other parameters constant at $\Psi_0 = 135°$, $L = 21$, $N = 32$, $K = 0.4$, $m = 100$, $\alpha = 1$, $\beta = 1$.
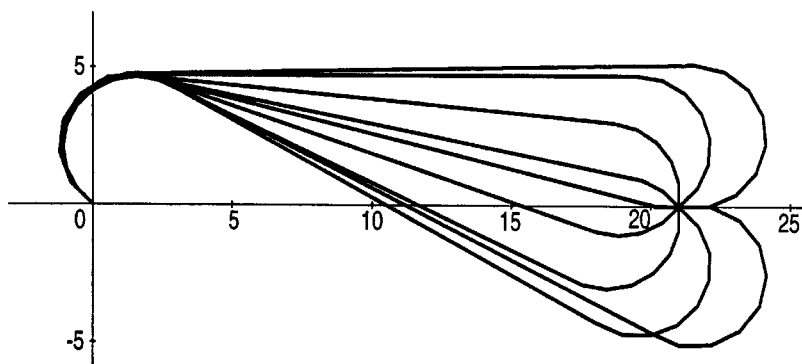
FIGURE 13   Minimal length curvature-limited curves with $m = 100$, $\Psi_0 = 135°$, $\Psi_N = -180°$, $-135°, \ldots, 180°$.
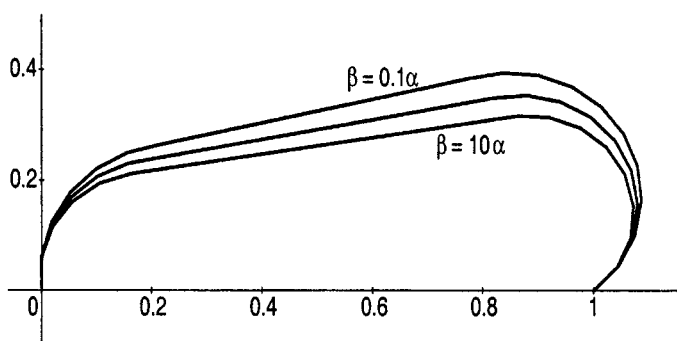
FIGURE 14   Curvature-limited elastica with $\Psi_0 = 90°, \Psi_N = -135°$, and $\beta/\alpha = 0.1, 1, 10$. The middle curve is the one obtained when $\beta = \alpha$.

Figure 14 shows the effect of α and β on the results when $m = 10$. As the ratio β/α increases, the length of the curve decreases, but to much less a degree than in Fig. 4 when m was 1. This phenomenon may be seen in Fig. 14, which shows curves for $\beta/\alpha = 0.1, 1.0$, and 10. When m gets larger the curves for different ratios of β/α resemble each other more closely. The other parameters are fixed at $\Psi_0 = 90°$, $\Psi_N = -135°$, $K = 6$, $L = 1$, and $N = 24$.

Figure 15 shows the effect on varying N, one less than the number of links, while holding the other parameters constant at $\Psi_0 = 90°$, $\Psi_N = 135°$, $K = 0.4$, $L = 12$, $m = 100$, $\alpha = 1$, $\beta = 1$. As expected, the curves converge to nearly a circle–line–circle path as N increases.
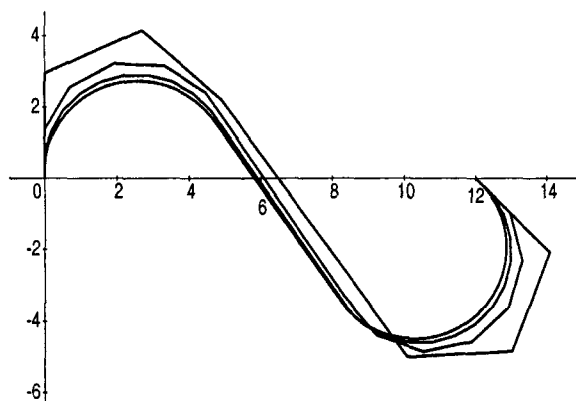
FIGURE 15   Minimal length curvature-limited elastica with varying N. From top to bottom at $x = 2$, these are the curves for $N = 8, 16, 32$, and 64 respectively.
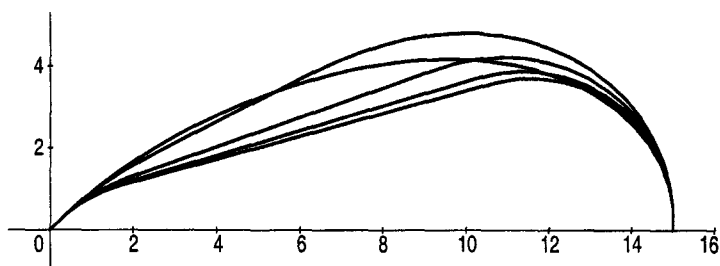
FIGURE 16   Minimal length curves for curvature-limited elastica with varying m. From top to bottom at $x = 8$, these are the curves for $m = 3, 1, 10, 30$, and 100 respectively.

Figure 16 shows the effect on varying m while holding the other parameters constant at $\Psi_0 = 45°$, $\Psi_N = -90°$, $K = 0.4$, $L = 15$, $N = 32$, $\alpha = 1$, $\beta = 1$. As m increases, the curves converge to a circle–line–circle path. There is little change in the curves once m is as large as 100.

5   SIMILARITY-INVARIANT TURN-LIMITED ELASTICA

As previously, we could set l to 1 and free the condition $l \sum_{i=0}^{N} \cos \Psi_i = L$ to $\sum_{i=0}^{N} \cos \Psi_i > 0$. However, this condition alone, in conjunction with a penalty function that allows all turns less

than K for free (almost – for high m's) could lead to some peculiar returns of the curve to the x-axis. Indeed, minimizing (5) with $l = 1$ and $\beta = 0$

$$\sum_{i=1}^{N}\left(\frac{\Psi_i - \Psi_{i-1}}{K}\right)^{2m}$$

subject to

$$\sum_{i=0}^{N} \sin \Psi_i = 0$$

leads to

$$\Psi_{j+1} = \Psi_j + \left[(\Psi_j - \Psi_{j-1})^{2m-1} + \lambda_2 \frac{K^{2m}}{2m} \cos \Psi_j\right]^{1/(2m-1)}.$$

Note however that as $m \to \infty$ the terms $[(\Psi_j - \Psi_{j-1})/K]^{2m}$ will all tend to zero if $|\Psi_j - \Psi_{j-1}| < K$, hence all sequences of Ψ_j obeying $|\Psi_j - \Psi_{j-1}| < K$ and $\sum_{i=0}^{N} \sin \Psi_i = 0$ will be equally good. Therefore to make the problem well defined we need to impose an additional constraint. With similarity invariance considerations in view, we require the minimization of

$$\sum_{i=1}^{N} \alpha \left(\frac{\Psi_i - \Psi_{i-1}}{K}\right)^{2m} + \frac{\beta}{\sum_{i=0}^{N} \cos \Psi_i} \tag{7}$$

subject to

$$\sum_{i=0}^{N} \sin \Psi_i = 0, \qquad \sum_{i=0}^{N} \cos \Psi_i > 0.$$

(Find interpolant with $l = 1$ and maximum L so that one has the greatest $L/[(N + 1)l]$ ratio.)

Lagrange multipliers were used to form the expression

$$\mathcal{F}(\Psi, \lambda; K, m, N, \alpha, \beta) = \alpha \sum_{i=1}^{N}\left(\frac{\Psi_i - \Psi_{i-1}}{K}\right)^{2m} + \frac{\beta}{\sum_{i=0}^{N} \cos \Psi_i} + \lambda \sum_{i=0}^{N} \sin \Psi_i.$$

Taking derivatives with respect to the N variables $\Psi_1, \ldots, \Psi_{N-1}$, and λ leads to this system which generalizes (4):

$$\frac{2m\alpha[(\Psi_j - \Psi_{j-1})^{2m-1} - (\Psi_{j+1} - \Psi_j)^{2m-1}]}{K^{2m}} + \frac{\beta \sin \Psi_j}{\left(\sum_{i=0}^{N} \cos \Psi_i\right)^2}$$

$$+\lambda \cos \Psi_j = 0, \quad j = 1, \ldots, N - 1, \quad \sum_{i=0}^{N} \sin \Psi_i = 0. \tag{8}$$

This optimization problem imposes the requirement to have $\sum_{i=0}^{N} \cos \Psi_i$, i.e. the excursion in the positive x-direction, as large as possible for a curve with given length $(N + 1)l$. This means that if we scale the curve so as to have $\Delta x = 1$, we shall have the polygonal curve of minimal length that obeys the (similarity invariant) local turn condition ($|\Psi_{j+1} - \Psi_j| < K$). Or, in other words, the curve with the best (total length)/(Δx-excursion) ratios among all interpolating curves with limited turn.

The problem with which we dealt in Section 4 has a continuous counterpart: an old result of Dubins (see [10]) states that minimal length curves with a constraint on the (average) curvature and prescribed initial and terminal positions and tangents are always composed of a circular arc (with radius determined by the maximum curvature allowed), a linear segment, and another circular arc (or a subset of these three pieces). As seen in the next section, the numerical method we developed indeed yielded (for high ms) such interpolants. In fact, this happened for both types of optimization problems considered above.

5.1   Numerical Experiments for Similarity-invariant Turn-limited Elastica

Here we want to solve the minimization problem (7). We wrote another Maple program to solve the corresponding system (8) for a wide range of parameter values. These were solved by a technique very similar to that described in detail in the previous section. The major difficulty arising in this case is that we do not know the value of L, or x_{N+1}, beforehand, so we cannot make the same computations

as before. However, we found that we obtained acceptable results when we made an initial guess based on the approximation $L \approx N$.

Figure 17 shows the effect on varying the terminal angle while holding the other parameters constant at $\Psi_0 = 135°$, $K = 0.4$, $m = 100$, $N = 32$, $\alpha = 1$, $\beta = 1$.

Figure 18 shows the same results as in Fig. 17, but with all of the distances scaled so that $L = x_{N+1} = 1$. This has the effect of changing l from 1 to $1/x_{N+1}$.
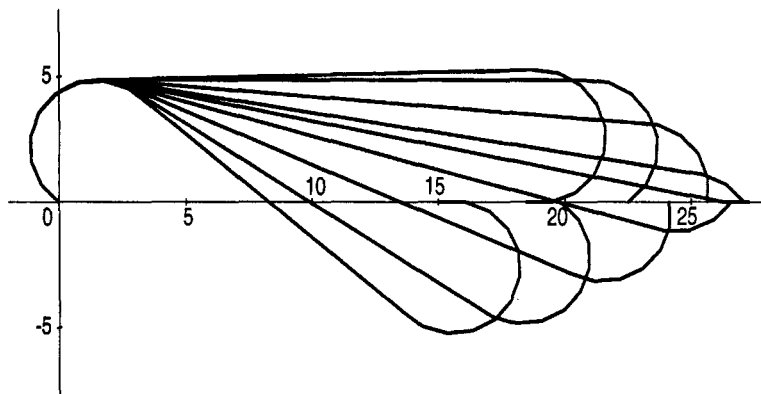
FIGURE 17   Maximal reach curves with $\Psi_0 = 135°$, $\Psi_N = -180°$, $-135°, \ldots, 180°$.
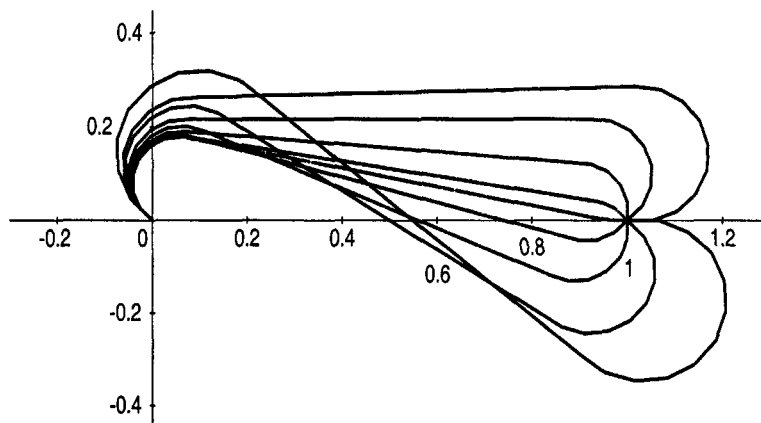
FIGURE 18   Normalized maximal reach (minimal length) curves with $\Psi_0 = 135°$, $\Psi_N = -180°$, $-135°, \ldots, 180°$.

Figure 19 shows the effect on varying m while holding the other parameters constant at $\Psi_0 = 90°$, $\Psi_N = -45°$, $K = 0.4$, $N = 16$, $\alpha = 1$, $\beta = 1$. As m increases, the curves converge to a circle–line–circle path. There is little change in the curves once m is as large as 100.

Figure 20 shows the same results as in Fig. 19, but with all of the distances scaled so that $x_{N+1} = 1$. Again, as m increases, the curves converge to a to a circle–line–circle path.
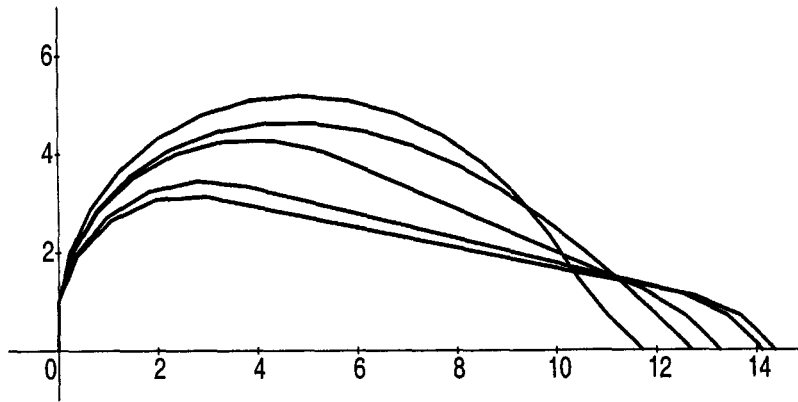
FIGURE 19   Minimal length curves for turn-limited elastica with varying m. From top to bottom at $x = 6$, these are the curves for $m = 3, 1, 10, 30$, and 100 respectively.
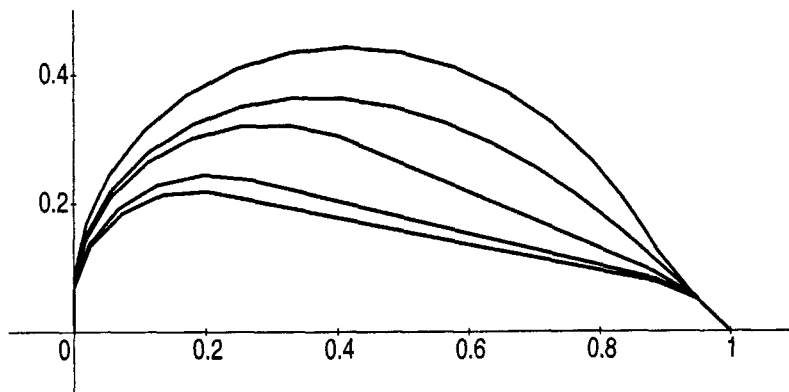
FIGURE 20   Normalized similarity-invariant elastica with varying m. From top to bottom at $x = 0.4$, these are the curves for $m = 3, 1, 10, 30$, and 100, respectively.

FIGURE 21   Similarity-invariant elastica with varying N. In order of increasing length, these are the curves for $N = 12, 24, 48$, and 96 respectively.
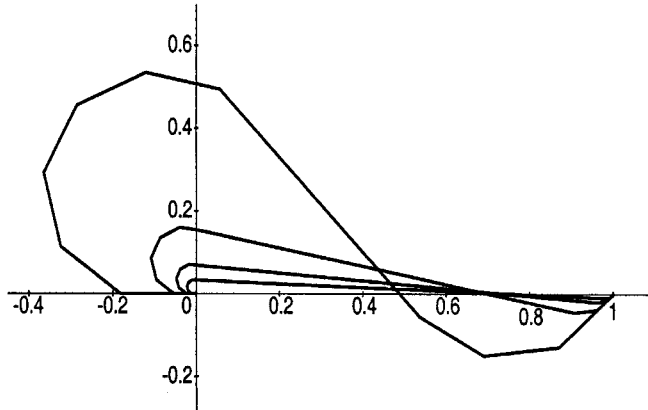
FIGURE 22   Normalized similarity-invariant elastica with varying N. From top to bottom at $x = 0.2$, these are the curves for $N = 12, 24, 48$, and 96 respectively.

Figure 21 shows the effect on varying N, one less than the number of links, while holding the other parameters constant at $\Psi_0 = 180°$ and $\Psi_N = 45°$, $K = 0.7$, $m = 100$, $\alpha = 1$, $\beta = 1$.

Figure 22 shows the same results as in Fig. 21, but with all of the distances scaled so that $x_{N+1} = 1$. The curves converge to nearly a circle–line–circle path since $m = 100$ here. Note however that since we do not adjust the turn parameter (K in this case is the maximum turn angle) at all, the limit of the curves will approach a straight line between two tiny circular arcs! To avoid this behavior we should tune K to the scale, but this would make our design dependent on an *a priori* knowledge of the scale.

6   DISCRETE MINIMUM VARIATION ELASTICA

In this section, following the suggestions of Moreton and Séquin [26] that minimum variation interpolation might lead to nicer curve

interpolations (in the continuous domain), we study cost functions of the form:

$$\text{Minimize} \quad \sum_i \left\{ \alpha \left[\frac{(\Psi_{i+1} - \Psi_i) - (\Psi_i - \Psi_{i-1})}{l^2} \right]^2 + \beta \right\} l$$

subject to

$\Psi_0, \theta_0, \Psi_N,$ and θ_{N+1} predetermined

$$\sum_{i=0}^{N} l \cos \Psi_i = L$$

$$\sum_{i=0}^{N} l \sin \Psi_i = 0$$

or the similarity-invariant version, where we minimize

$$\sum_i [(\Psi_{i+1} - \Psi_i) - (\Psi_i - \Psi_{i-1})]^2,$$

after having set $l = 1$ and relinquishing the requirement that the poly-line terminate at a specific point on the x-axis. By predetermining θ_0 and θ_{N+1} we mean that we wish to specify rates of change of Ψ at the endpoints $(0,0)$ and $(L,0)$, respectively. This is equivalent to adding two points P_{-1} and P_{N+2} to the path so that Ψ_{-1}, the angle between $\overline{P_{-1}P_0}$ and $\overline{P_0P_1}$, satisfies $\Psi_{-1} = \Psi_0 - \theta_0$, and Ψ_{N+1}, the angle between $\overline{P_NP_{N+1}}$ and $\overline{P_{N+1}P_{N+2}}$, satisfies $\Psi_{N+1} = \Psi_N + \theta_{N+1}$.

6.1 Euclidean-invariant Minimum Variation Elastica

With the above understanding, the Euclidean-invariant minimization problem takes the form

$$\text{Minimize} \quad \sum_{i=0}^{N} \left[\alpha \left(\frac{\Psi_{i+1} - 2\Psi_i + \Psi_{i-1}}{l^2} \right)^2 + \beta \right] l \tag{9}$$

subject to

$\Psi_{-1}, \Psi_0, \Psi_N,$ and Ψ_{N+1} predetermined

$$\sum_{i=0}^{N} l \cos \Psi_i = L$$

$$\sum_{i=0}^{N} l \sin \Psi_i = 0.$$

Lagrange multipliers were used to form the expression

$$\mathcal{G}(\mathbf{\Psi}, \lambda_1, \lambda_2, l; L, N, \alpha, \beta) = \alpha l \sum_{i=0}^{N} \left(\frac{\Psi_{i+1} - 2\Psi_i + \Psi_{i-1}}{l^2} \right)^2 + N\beta l$$

$$+ \lambda_1 \left(l \sum_{i=0}^{N} \cos \Psi_i - L \right) + \lambda_2 l \sum_{i=0}^{N} \sin \Psi_i,$$

where $\mathbf{\Psi}$ denotes the vector of unknown angles $\{\Psi_1, \ldots, \Psi_{N-1}\}$. Taking derivatives with respect to the $N + 2$ variables $\Psi_1, \ldots, \Psi_{N-1}$, λ_1, λ_2, and l, leads to the system of equations

$$\left. \begin{array}{c} \dfrac{2\alpha(\Psi_{j+2} - 4\Psi_{j-1} + 6\Psi_j - 4\Psi_{j-1} + \Psi_{j-2})}{l^4} - \lambda_1 \sin \Psi_j + \lambda_2 \cos \Psi_j = 0, \\[2mm] j = 1, \ldots, N - 1, \\[2mm] l \displaystyle\sum_{i=0}^{N} \cos \Psi_i - L = 0, \quad \displaystyle\sum_{i=0}^{N} \sin \Psi_i = 0, \\[2mm] -3\alpha \displaystyle\sum_{i=0}^{N} \left(\dfrac{\Psi_{i+1} - 2\Psi_i + \Psi_{i-1}}{l^2} \right)^2 + (N+1)\beta \\[2mm] + \lambda_1 \displaystyle\sum_{i=0}^{N} \cos \Psi_i + \lambda_2 \displaystyle\sum_{i=0}^{N} \sin \Psi_i = 0. \end{array} \right\}$$

(10)

This leads to a system of equations for the Ψ_j sequence of the form

$$\Psi_{j+2} - 4\Psi_{j+1} + 6\Psi_j - 4\Psi_{j-1} + \Psi_{j-2}$$

$$+ \frac{3}{2} \frac{\sum_{i=0}^{N} (\Psi_{i+1} - 2\Psi_i + \Psi_{i-1})^2}{(N-1)\beta + \lambda_1 \sum_{i=0}^{N} \cos \Psi_i + \lambda_2 \sum_{i=0}^{N} \sin \Psi_i} [\lambda_1 \sin \Psi_j - \lambda_2 \cos \Psi_j] = 0,$$

$$j = 1, \ldots, N - 1,$$

with Ψ_{-1}, Ψ_0, Ψ_N, and Ψ_{N+1} predetermined.

6.1.1   Numerical Experiments with Euclidean-invariant Minimum Variation Elastica

In this section and in Section 6.2.1 we discuss in detail the various problems and the numerical solutions corresponding to the cost functions described in Section 6. We also show several families of curves illustrating how changing some of the parameters affects the minimal cost curves for the various cost functions. In all of the examples in this section we take $\theta_0 = \theta_{N+1} = 0$, or equivalently $\Psi_{-1} = \Psi_0$ and $\Psi_{N+1} = \Psi_N$, so that the instantaneous change in curvature at each endpoint is zero.

The discrete Euclidean-invariant minimum variation elastica curves are solutions of the optimization problem (9). Solving the system (10) and the corresponding system (12) in the next section proved to be more difficult than for those in Section 5, due to the difficulty of obtaining a good initial guess. The same type of Newton–Raphson method as before was used, but for some specific problems the initial guess had to be individually tailored. An initial guess which worked quite often was that in which $\Psi_1 = \Psi_0 - KL/N$, $\Psi_2 = \Psi_1 - 2KL/N$, $\Psi_{N-1} = \Psi_N \pm KL/N$, $\Psi_{N-2} = \Psi_{N-1} \pm 2KL/N$, and the remaining Ψ_i all equal to the arctangent of the slope of the line segment joining $\mathbf{P}_2$ and $\mathbf{P}_{N-2}$ obtained in this manner, with the upper of the $\pm$ symbols used when $\Psi_N < 0$ and the lower sign when $\Psi_N \geq 0$.

Figure 23 shows the effect on varying the terminal angle while holding the other parameters constant at $\Psi_0 = 135°$, $L = 10$, $N = 32$, $\alpha = 1$, $\beta = 1$.

Figure 24 shows the effect of α and β on the results. As the ratio β/α increases, the contribution of the length of the curve to the cost function increases, and as a result the length of the curve decreases. This phenomenon is readily seen in Fig. 24, which shows curves for $\beta/\alpha = 0.1, 1.0$, and 10. The other parameters are fixed at $\Psi_0 = 180°$, $\Psi_N = 180°$, $L = 10$, and $N = 32$. Note that, in comparison with Fig. 4, minimizing β, i.e. removing the penalty on total length, does not have as dramatic an effect here as in the case where the length was balanced against the integrated squared curvature.

Figure 25 shows the effect on varying N, one less than the number of links, while holding the other parameters constant at $\Psi_0 = 45°$, $\Psi_N = -135°$, $L = 6$, $\alpha = 1$, $\beta = 1$. In this case there is very little change in the curve for values of N larger than 16.
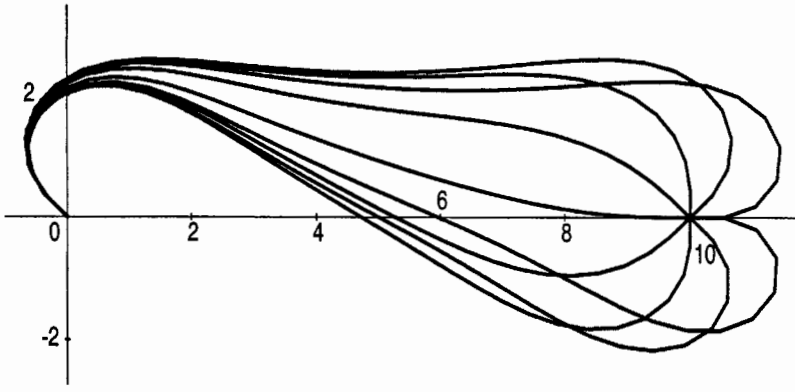
FIGURE 23   Discrete Euclidean minimum variation elastica with $\Psi_0 = 135°$, $\Psi_N = -180°, -135°, \ldots, 180°$.
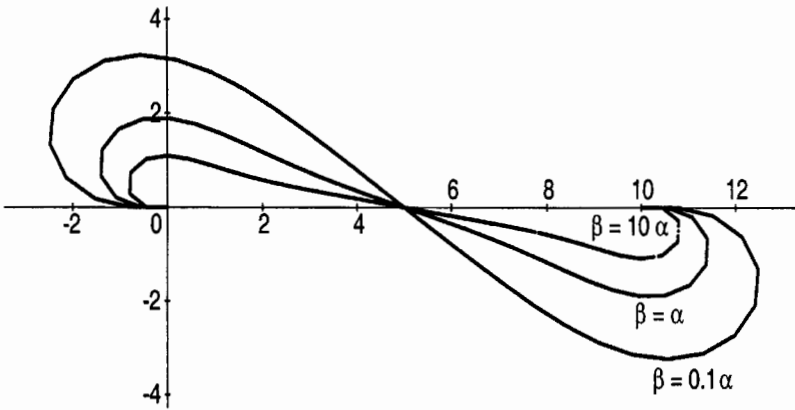
FIGURE 24   Discrete Euclidean minimum variation elastica with $\Psi_0 = 180°$, $\Psi_N = 180°$, and $\beta/\alpha = 0.1, 1, 10$.

6.2   Similarity-invariant Minimum Variation Elastica

With the understanding of Section 6, the similarity-invariant minimization problem takes the form

$$\text{Minimize } \sum_{i=0}^{N} \alpha(\Psi_{i+1} - 2\Psi_i + \Psi_{i-1})^2 + \frac{\beta}{\sum_{i=0}^{N} \cos \Psi_i} \qquad (11)$$
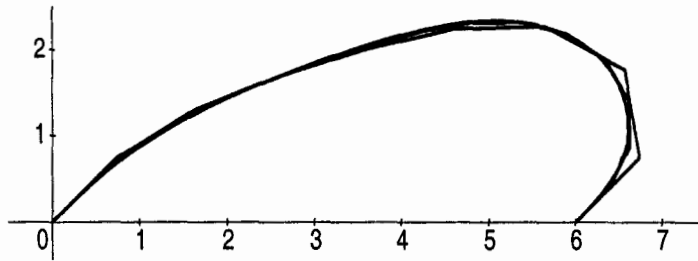
FIGURE 25 Discrete Euclidean minimum variation elastica with varying N. From bottom to top at $x = 5$, these are the curves for $N = 8, 16, 32$, and 64 respectively.

subject to

$$\Psi_{-1}, \Psi_0, \Psi_N, \text{ and } \Psi_{N+1} \text{ predetermined}$$

$$\sum_{i=0}^{N} l \cos \Psi_i = L$$

$$\sum_{i=0}^{N} l \sin \Psi_i = 0.$$

(i.e. the problem of finding the interpolant with $l = 1$ and maximum L, so that one has the largest $L/[(N + 1)l]$ ratio).

Lagrange multipliers were used to form the expression

$$\mathcal{F}(\Psi, \lambda; N, \alpha, \beta) = \alpha \sum_{i=0}^{N} (\Psi_i - \Psi_{i-1})^2 + \frac{\beta}{\sum_{i=0}^{N} \cos \Psi_i} + \lambda \sum_{i=0}^{N} \sin \Psi_i,$$

where Ψ denotes the vector of unknown angles $\{\Psi_1, \ldots, \Psi_{N-1}\}$. Taking derivatives with respect to the N variables $\Psi_1, \ldots, \Psi_{N-1}$, and λ leads to this system:

$$2\alpha(\Psi_{j+2} - 4\Psi_{j+1} + 6\Psi_j - 4\Psi_{j-1} + \Psi_{j-2}) + \frac{\beta \sin \Psi_j}{\left(\sum_{i=0}^{N} \cos \Psi_i\right)^2}$$

$$+ \lambda \cos \Psi_j = 0, \quad j = 1, \ldots, N - 1, \tag{12}$$

$$\sum_{i=0}^{N} \sin \Psi_i = 0.$$

6.2.1 Numerical Experiments with Similarity-invariant Minimum Variation Elastica

The discrete similarity-invariant minimum variation elastica curves are solutions of the optimization problem (11). The system (12) was solved by a technique very similar to that in the previous section. As in Section 5.1, since we do not know the value of L, or x_{N+1}, beforehand, we used an initial guess based on the approximation $L \approx N$.

Figure 26 shows the effect on varying the terminal angle while holding the other parameters constant at $\Psi_0 = 135°$, $N = 32$, $\alpha = 1$, $\beta = 1$.

Figure 27 shows the same results as in Fig. 26, but with all of the distances scaled so that $L = x_{N+1} = 1$. This has the effect of changing l from 1 to $1/x_{N+1}$.

Figure 28 shows the effect on varying β/α while holding the other parameters constant at $\Psi_0 = 90°$, $\Psi_N = -45°$, $N = 32$. As in Figs 14 and 24, as β/α increases from 0.1 to 1 to 10, so does x_{N+1}, the "reach" of the curve.

Figure 29 shows the same results as in Fig. 28, but with all of the distances scaled so that $x_{N+1} = 1$.
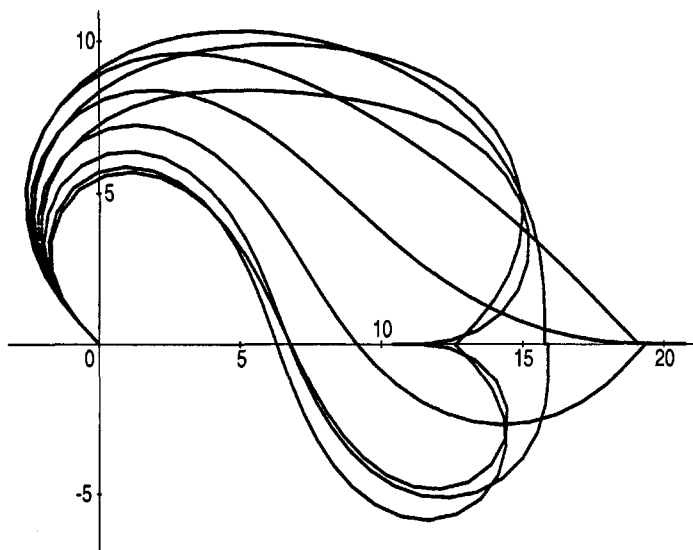
FIGURE 26   Maximal reach minimum variation curves with $\Psi_0 = 135°$, $\Psi_N = -180°$, $-135°$, ..., $180°$.
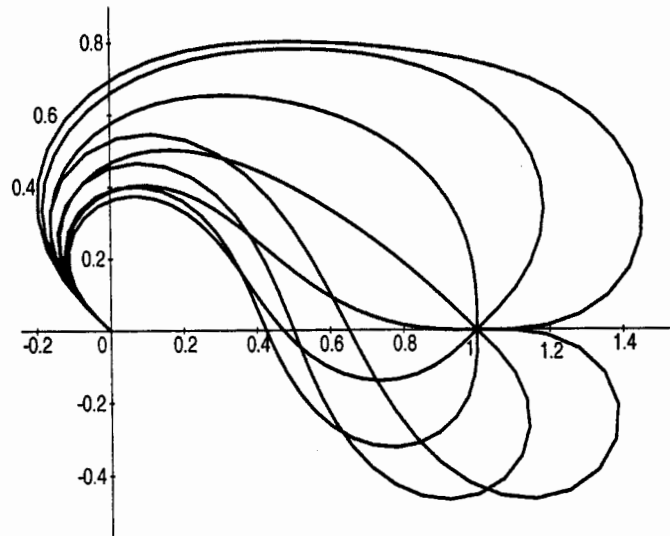
FIGURE 27   Normalized maximal reach (minimal length) minimum variation curves
with $\Psi_0 = 135°, \Psi_N = -180°, -135°, \ldots, 180°$.
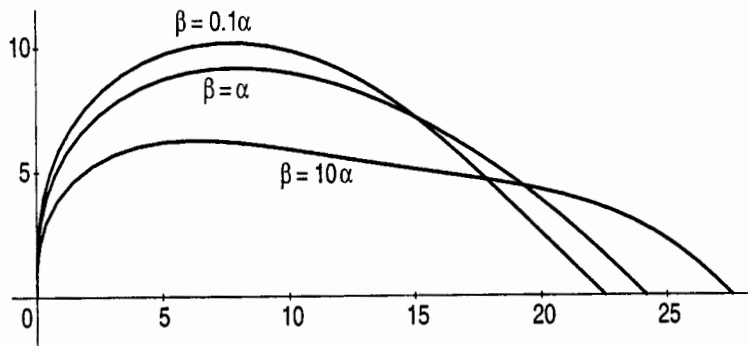
FIGURE 28   Discrete similarity-invariant minimum variation elastica with $\Psi_0 = 45°$,
$\Psi_N = -135°$, and $\beta/\alpha = 0.1, 1, 10$.

Figure 30 shows the effect on varying N, one less than the number
of links, while holding the other parameters constant at $\Psi_0 = 180°$ and
$\Psi_N = 45°, \alpha = 1, \beta = 1$.

Fig. 31 shows the same results as in Fig. 30, but with all of the dis-
tances scaled so that $x_{N+1} = 1$.
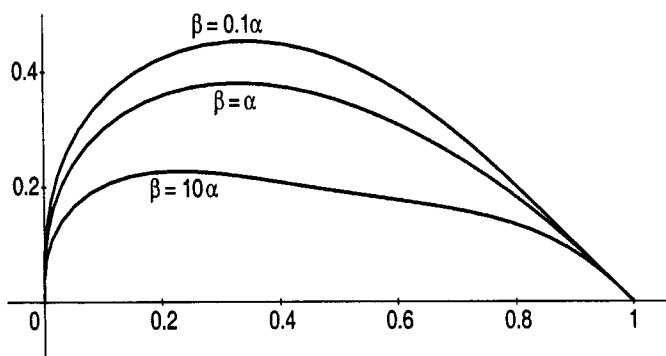
FIGURE 29   Normalized discrete similarity-invariant minimum variation elastica
with $\Psi_0 = 45°$, $\Psi_N = -135°$, and $\beta/\alpha = 0.1, 1, 10$.
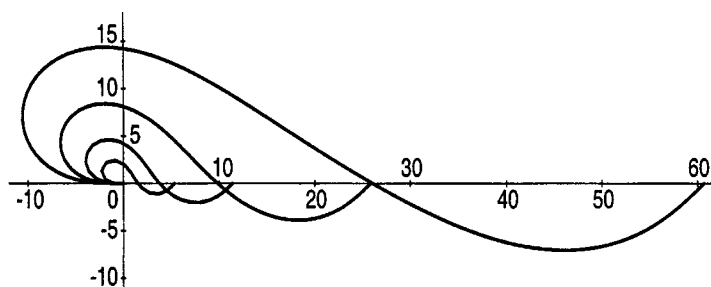
FIGURE 30   Similarity-invariant minimum variation elastica with varying N. In
order of increasing length, these are the curves for $N = 12, 24, 48$, and 96 respectively.
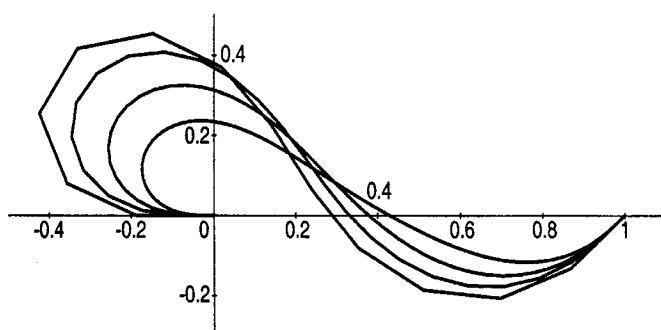
FIGURE 31   Normalized similarity-invariant minimum variation elastica with vary-
ing N. From bottom to top at $x = 0.6$, these are the curves for $N = 12, 24, 48$, and 96
respectively.

7 CONCLUSIONS

We have introduced and discussed discrete versions of "minimal energy" and "minimum curvature variation" curve designs. We claim the discretizations provide excellent approximations to the continuous problems and may be very useful for a variety of CAD applications. Of course, other types of cost functions could and should be considered within the same framework.

The numerical work showed that the Newton–Raphson method was suitable for a wide variety of such problems, especially since good initial guesses could be provided, using the anticipated behavior of results stemming from theoretical studies of the continuous versions of the problems. A good initial guess was especially critical in the cases where the curvature penalty function approached a barrier function (not unexpectedly!). Extensions and comparisons to other numerical approaches are currently under investigation.

Whenever one proposes the consideration of a discretized model rather than the discretization of the continuous solutions of continuous models, the question of convergence of the discrete to the continuum arises. In the context of discretized elastica as proposed herein, it was found that the theory of Γ-convergence dealing with discrete approximations of continuous functionals in the context of variational calculus is applicable here. The Γ-convergence proofs is the subject of a companion paper [4].

References

[1] C.L. Bajaj and G. Xu (1994). NURBS approximation of surface/surface intersection curves. *Advances in Computational Mathematics*, **2**, 1–21.
[2] M. Born (1906). Stabilität der elastischen Linie in Ebene und Raum. PhD thesis, Göttingen, Göttingen, Germany.
[3] A.M. Bruckstein and A.N. Netravali (1990). On minimal energy trajectories, *Computer Vision, Graphics, and Image Processing*, **49**, 283–296.
[4] A.M. Bruckstein, A.N. Netravali and T.J. Richardson (2001). Epi-convergence of discrete elastica. *Applicable Analysis*, **77**.
[5] G. Brunnett and J. Wendt (1997). A univariate method for plane elastic curves. *Computer Aided Geometric Design*, **14**, 273–292.
[6] G. Brunnett and J. Wendt (1998). Elastic splines with tension control. In: M. Daehlen, T. Lyche and L.L. Schumaker (Eds.), *Mathematical Methods for Curves and Surfaces II*, pp. 33–40, Vanderbilt University Press, Nashville, TN.
[7] R. Bryant and P. Griffiths (1986). Reduction for constrained variational problems and $\int (\kappa^2/2)\,ds$. *American Journal of Mathematics*, **108**, 525–570.

[8] B.W. Char, K.O. Geddes, G.H. Gonnet, M.B. Monagan and S.M. Watt (1990). *Maple V User's Guide*. Watcom Publications Limited, Waterloo, Ontario.

[9] I.D. Cooper (1992). Curve interpolation with nonlinear spiral splines. *IMA Journal of Numerical Analysis*, **13**, 327–341.

[10] L.E. Dubins (1957). On curves of minimal length with a constraint on average curvature, and with prescribed initial and terminal positions and tangents. *American Journal of Mathematics*, **79**, 497–516.

[11] J.A. Edwards (1992). Exact equations of the nonlinear spline. *ACM Transactions on Mathematical Software*, **18**, 174–192.

[12] L. Euler (1744). Additamentum De Curvis Elasticis. In *Methodus Inveniendi Lineas Curvas Maximi Minimive Proprietate Gaudentes*, Lausanne.

[13] G. Farin (1990). *Curves and Surfaces for Computer Aided Geometric Design: A Practical Guide*. Academic Press, Boston.

[14] D.R. Ferguson and T.A. Grandine (1990). On the construction of surface interpolating curves. *ACM Transactions on Graphics*, **9**, 212–225.

[15] K. Foltinek (1994). The Hamiltonian theory of elastica. *American Journal of Mathematics*, **116**, 1479–1488.

[16] M. Golomb and J. Jerome (1982). Equilibria of the curvature functional and manifolds of nonlinear interpolating spline curves. *SIAM Journal of Mathematical Analysis*, **13**, 421–458.

[17] B.K.P. Horn (1983). The curve of least energy. *ACM Transactions on Mathematical Software*, **9**, 441–460.

[18] E. Jou and W. Han (1990). Minimal-energy splines: I. Plane curves with angle constraints. *Mathematical Methods in the Applied Sciences*, **13**, 351–372.

[19] E. Jou and W. Han (1992). Minimal-energy splines with various end constraints. In: H. Hagen, (Ed.), *Curve and Surface Design*, pp. 23–40. SIAM, Philadelphia.

[20] V. Jurdjevic (1995). Non-Euclidean elastica. *American Journal of Mathematics*, **117**, 93–124.

[21] M. Kallay (1986). Plane curves of minimal energy. *ACM Transactions on Mathematical Software*, **12**, 219–222.

[22] M. Kallay (1987). Method to approximate the space curve of least energy and prescribed length. *Computer-Aided Design*, **19**, 73–76.

[23] E.H. Lee and G.E. Forsythe (1973). Variational study of nonlinear spline curves. *SIAM Review*, **15**, 120–133.

[24] A.E.H. Love (1927). *The Mathematical Theory of Elasticity*. Cambridge University Press, London.

[25] M. Malcolm (1977). On the computation of nonlinear spline functions. *SIAM Journal of Numerical Analysis*, **14**, 254–282.

[26] H.P. Moreton and C.H. Séquin (September 1993). Scale-invariant minimum-cost curves: Fair and robust design implements. In: *Proceedings of Eurographics 93*, Barcelona, C-473–C-484.

[27] M.E. Mortensen (1985). *Geometric Modeling*, John Wiley & Sons, New York.

[28] D. Mumford (1994). Elastica and computer vision. In: C.L. Bajaj, (Ed.), *Algebraic Geometry and its Applications*, pp. 491–506. Springer-Verlag, New York.

[29] D.B. Parkinson and D.N. Moreton (1991). Optimal biarc-curve fitting. *Computer-Aided Design*, **23**, 411–419.

[30] W.S. Rutkowski (1979). Shape completion. *Computer Graphics and Image Processing*, **9**, 89–101.

[31] S. Ullman (1976). Filling in the gaps: The shape of subjective contours and a model for their generation. *Biological Cybernetics*, **25**, 1–6.